Synthetic Modeling for an Acoustic Exploration System for Physical Oceanography

BERTA BIESCAS,* BARRY RUDDICK,+ JEAN KORMANN,# VALENTÍ SALLARÈS,@ MLADEN R. NEDIMOVIĆ,& AND SANDRO CARNIEL**

* *Istituto di Scienze Marine, CNR, Bologna, Italy*
+ *Department of Oceanography, Dalhousie University, Halifax, Nova Scotia, Canada*
# *Barcelona Supercomputing Center, Barcelona, Spain*
@ *Department of Marine Geosciences, Institute of Marine Sciences, Barcelona, Spain*
& *Department of Earth Sciences, Dalhousie University, Halifax, Nova Scotia, Canada*
** *Istituto di Scienze Marine, CNR, Venice, Italy*

(Manuscript received 3 July 2015, in final form 9 November 2015)

ABSTRACT

Marine multichannel seismic (MCS) data, used to obtain structural reflection images of the earth's subsurface, can also be used in physical oceanography exploration. This method provides vertical and lateral resolutions of $O(10–100)$ m, covering the existing observational gap in oceanic exploration. All MCS data used so far in physical oceanography studies have been acquired using conventional seismic instrumentation originally designed for geological exploration. This work presents the proof of concept of an alternative MCS system that is better adapted to physical oceanography and has two goals: 1) to have an environmentally low-impact acoustic source to minimize any potential disturbance to marine life and 2) to be light and portable, thus being installed on midsize oceanographic vessels. The synthetic experiments simulate the main variables of the source, shooting, and streamer involved in the MCS technique. The proposed system utilizes a 5-s-long exponential chirp source of 208 dB relative to 1 μPa at 1 m with a frequency content of 20–100 Hz and a relatively short 500-m-long streamer with 100 channels. This study exemplifies through numerical simulations that the 5-s-long chirp source can reduce the peak of the pressure signal by 26 dB with respect to equivalent air gun–based sources by spreading the energy in time, greatly reducing the impact to marine life. Additionally, the proposed system could be transported and installed in midsize oceanographic vessels, opening new horizons in acoustic oceanography research.

1. Introduction

The main physical parameters of the ocean (temperature, salinity, pressure, and density) are traditionally measured using vertical profiles as conductivity–temperature–depth (CTD) casts or expendable bathythermographs (XBT). These instruments sample the ocean at a vertical resolution of $O(0.1–1)$ m, which allows analysis of processes generated within the submesoscale and finescale. However, this method of exploration does not observe lateral structure at these scales because typical lateral distances between vertical casts are rarely shorter than $O(10^3)$ m. This observational gap is becoming increasingly relevant as numerical models increase in resolution. Physical oceanographers demand empirical data with a lateral resolution of $O(10–100)$ m to calibrate and validate new models and theory (e.g., Ruddick 2003; Smith and Ferrari 2009; Hua et al. 2013).

Marine multichannel seismic reflection (MCS) data, collected and used to obtain structural images of the earth's subsurface, also display coherent reflections from within the water layer. A partial list of features observed via MCS data includes internal waves, thermohaline staircases and intrusions, density and turbidity currents, and submesoscale coherent vortices, which are key ocean mixing processes (e.g., Biescas et al. 2008; Ménesguen et al. 2009; Pinheiro et al. 2010; Biescas et al. 2010; Quentel et al. 2010; Vsemirnova et al. 2012; Holbrook et al. 2013). Because of the signal redundancy provided by the multiple illumination of a single reflector point, MCS systems enhance coherent signals over noise, resulting in clear acoustic images of the oceanic thermohaline structure with lateral and vertical resolutions of

Corresponding author address: Berta Biescas, Istituto di Scienze Marine, CNR, Via Gobetti 101, 40129 Bologna, Italy.
E-mail: berta.biescas@ve.ismar.cnr.it

DOI: 10.1175/JTECH-D-15-0137.1

TABLE 1. Parameters used in the synthetic modeling codes. The Ricker wavelet follows the equation $\text{RickerSource}(t) = A[1-2\pi f_0(t-t_0)^2]\exp[-\pi f_0(t-t_0)^2]$, where $f_0 = 45$ Hz and $t_0 = 0.33$ s. The chirp wavelet follows the equation $\text{ChirpSource}(t) = A\exp[-(t-t_0/2)^2]\sin\{\phi + [2\pi f_1(k^t-1)/lnk]\}$, where $t_0 = 2.5$ s, $k = (f_2/f_1)^{1/t_{max}}$, $f_1 = 20$ Hz, $f_2 = 100$ Hz, $t_{max} = 5$ s, and $\phi = 0$. The acoustic media used in both simulations is the inverted sound speed grid from the GO-LR-01 profile (Biescas et al. 2014).

Parameter	Ricker	Chirp
Frequency content	10–100 Hz	20–100 Hz
Peak-to-peak amplitude	234 dB relative to 1 μPa at 1 m	210 dB relative to 1 μPa at 1 m
Depth of the source	9 m	9 m
Depth of the streamer	8 m	8 m
Grid spacing of the model	1.56 m	1 m
Distance between receivers	12.5 m	5 m
Distance between shots	20 m	20 m
First offset	84 m	84
Number of channels	192	100
PML layers	106	106

O(1–100) m. Furthermore, inversion methods applied to acoustic images provide 2D temperature and salinity maps, which may cover the current observational gap in physical oceanography exploration (Papenberg et al. 2010; Bornstein et al. 2013; Biescas et al. 2014).

All MCS surveys carried out so far for oceanic research have used conventional seismic instrumentation (air gun sources and hydrophone streamers) and standard acquisition parameters (shot spacing, distance between channels, source power, etc.) that were conceived for geological exploration. However, oceanic targets are shallower, typically from the sea surface to 4 km deep, and their exploration does not require the same source characteristics as for geological exploration.

This work presents an alternative MCS system adapted for physical oceanography exploration using a methodology for generating synthetic MCS experiments in the ocean. The goal is to have an environmentally low-impact system with the weakest possible source in order to minimize any potential disturbance to marine life that can be installed in midsize oceanographic vessels. The proposed system is simulated using a numerical solver of the acoustic wave equation, acoustic ambient noise in the ocean, and a realistic model of the water layer. The system is based on chirp signals, which are commonly used to examine the sediments on and below the seafloor. Impulsive sources, such as air guns, emit high peak pressures in a very short time ($\sim 10^{-3}$ s); on the contrary, chirp signals spread the source energy out over time, reducing the peak sound levels.

In section 2, the methodology used to model the synthetic MCS experiment, generating synthetic shot gathers and synthetic oceanic noise is detailed. In section 3, stack sections of two synthetic experiments are presented. The first simulation uses similar parameters to a seismic oceanography experiment carried out in the northeastern Atlantic Ocean during the geophysical oceanography (GO) survey in 2006 (Hobbs et al. 2009). The comparison between the record sections obtained with the air gun source and acquisition parameters used in the GO experiment and the real data allows us to validate our methodology. The second simulation corresponds to the proposed portable system, which uses a 5-s-long exponential chirp wavelet of 208 dB relative to 1 μPa at 1 m and a relatively short 500-m-long streamer with 100 channels. In the last section, a discussion and conclusions are presented.

2. Methodology

The methodology used to generate the synthetic experiments consists of the following main steps: first, the shot gathers are generated using a 2D finite-difference algorithm that solves the acoustic wave equation [Eq. (3)] within a grid that represents the oceanic properties. The grid representing the ocean corresponds to a model of properties that was obtained by inversion of real MCS data along profile GO-LR-01 of the GO experiment (Biescas et al. 2014) and contains sound speed values with vertical and lateral resolutions of 10 and 100 m, respectively. The sound speed model was discretized to solve the acoustic wave equation with the parameters shown in Table 1. In our modeling approach, we did not take into account density because the contribution of this parameter to reflectivity is minor in comparison to the contribution of the sound speed (Sallarès et al. 2009) and it does not affect the main conclusions of the work. The location of the source moves along the top of the grid in accordance to the shot spacing. For each shot gather, the acoustic wave field is recorded and saved at the position of each channel of the streamer. Once shot gathers for the whole line are generated, background oceanic noise is added to the synthetic shot gathers. The simulated noisy synthetic shot gathers are then

processed using standard MCS functions to obtain the stacked section. Finally, the quality of the tested MCS system is quantified by measuring the spectral signal-to-noise ratio (SNR) in the stack section.

a. Acoustic source

Two different wavelets are used in the simulations presented in this work: (i) a Ricker wavelet of 234 dB relative to 1 μPa at 1 m with a frequency content within the range of 10–100 Hz, which is similar to the wavelet produced by the source used in the GO-LR-01 profile of the GO survey and is used to calibrate the synthetic simulations; and (ii) a 5-s-long exponential chirp wavelet (Flandin 2001) of 208 dB relative to 1 μPa at 1 m amplitude, a Gaussian taper, and a frequency content of 20–100 Hz. The Ricker and the chirp wavelets are described by the following equations:

$$\text{RickerSource}(t) = A[1 - 2\pi f_0 (t - t_0)^2] \exp[-\pi f_0 (t - t_0)^2], \tag{1}$$

where $A = 500\,000$ is the maximum amplitude of the wavelet, $f_0 = 45$Hz, and $t_0 = 0.33$ s;

$$\text{ChirpSource}(t) = A \exp\left[-\left(\frac{t - t_0}{2}\right)^2\right] \sin\left\{\phi + \left[2\pi f_1 \frac{(k^t - 1)}{lnk}\right]\right\}, \tag{2}$$

where $A = 25\,000$ is the maximum amplitude of the wavelet, $\exp[-(t - t_0)^2]$ with $t_0 = 2.5$ s corresponds to a 5-s-wide Gaussian taper, $k = (f_2/f_1)^{1/t_{\max}}$, $t_{\max} = 5$ s, $\phi = 0$, $f_1 = 20$ Hz, and $f_2 = 100$ Hz. The wavelets, frequency content, and frequency change in time are shown in Fig. 1.

b. Synthetic shot gather generation and MCS processing

A 2D finite-difference time-domain (FDTD) algorithm with high-order spatial discretization is used to solve the acoustic wave equation [Eq. (3)] and simulate the wave propagation through the ocean,

$$\nabla^2 p - \frac{1}{c^2} \frac{\partial^2 p}{t\partial^2} + f_s = 0, \tag{3}$$

where f_s is the source function, p is the pressure, and c is the sound speed. The code includes second-order perfectly matched layers (PML) specifically designed for Seismic Oceanography simulations for the bottom and side lateral boundaries, while a free-surface condition is introduced at the top boundary by setting $p = 0$ at $z = 0$. This code was previously presented and validated by Kormann et al. (2009, 2010). The variables included are wavelet type, wavelet frequency content, wavelet amplitude, depth and spacing of the acoustic source; number of channels or receiver groups, distance between them, near offset and depth of the streamer; recording time; acoustic media sound speed, grid spacing, and PML layer for absorbing boundaries. Specific values used in the modeling are detailed in Table 1. Once the shot gathers are generated by recording the data at the positions defined by channel locations along the streamer (Fig. 2a), the synthetic noise is added to each channel and shot (Fig. 2b); and finally, standard MCS processing is applied, consisting of frequency filter, spherical divergence correction, normal move-out (NMO) correction with a constant velocity, and common midpoint (CMP) sort and stack (Fig. 2c). The chirp simulation has an additional step in which the data trace from each channel is correlated with the chirp function (from Fig. 2e to Fig. 2f). The stack from the real data corresponding to the GO experiment (Fig. 4a) is obtained by applying the same processing flow. Seismic UNIX (Cohen and Stockwell 2003) was used for the MCS processing.

c. Streamer and fold

Since reflection coefficients in oceanic water are $O(10^{-4})$, the fine structure reflectivity is only weakly detected in a single channel, unless powerful sources are used (e.g., the source used in the Iberian–Atlantic Margin Survey, ~240 dB relative to 1 μPa at 1 m; Buffett et al. 2009). However, a key characteristic of MCS systems that makes them capable of detecting the oceanic fine structure is the CMP method (Yilmaz 2001), which records echoes from the same reflection point multiple times from different angles. The SNR increase is achieved during data processing, when the recorded signals reflected from the same subsurface locations and found in the same CMP are summed (''stacked'' in seismic processing terminology). The SNR increases because the amplitudes of the reflections add coherently, unlike the background noise, which is random in nature and therefore diminished. The CMP fold is the number of signals that are summed. It is proportional to the number of channels in the streamer and inversely proportional to the shot spacing:

$$\begin{aligned}\text{minfold} &= \frac{\text{num channels} \times \text{distance between channels}}{2 \times \text{distance between shots}} \\ &= \frac{\text{streamer length}}{2 \times \text{distance between shots}}\end{aligned} \tag{4}$$

Even though the above-mentioned expression defines the minimum fold, it can be arbitrary increased by

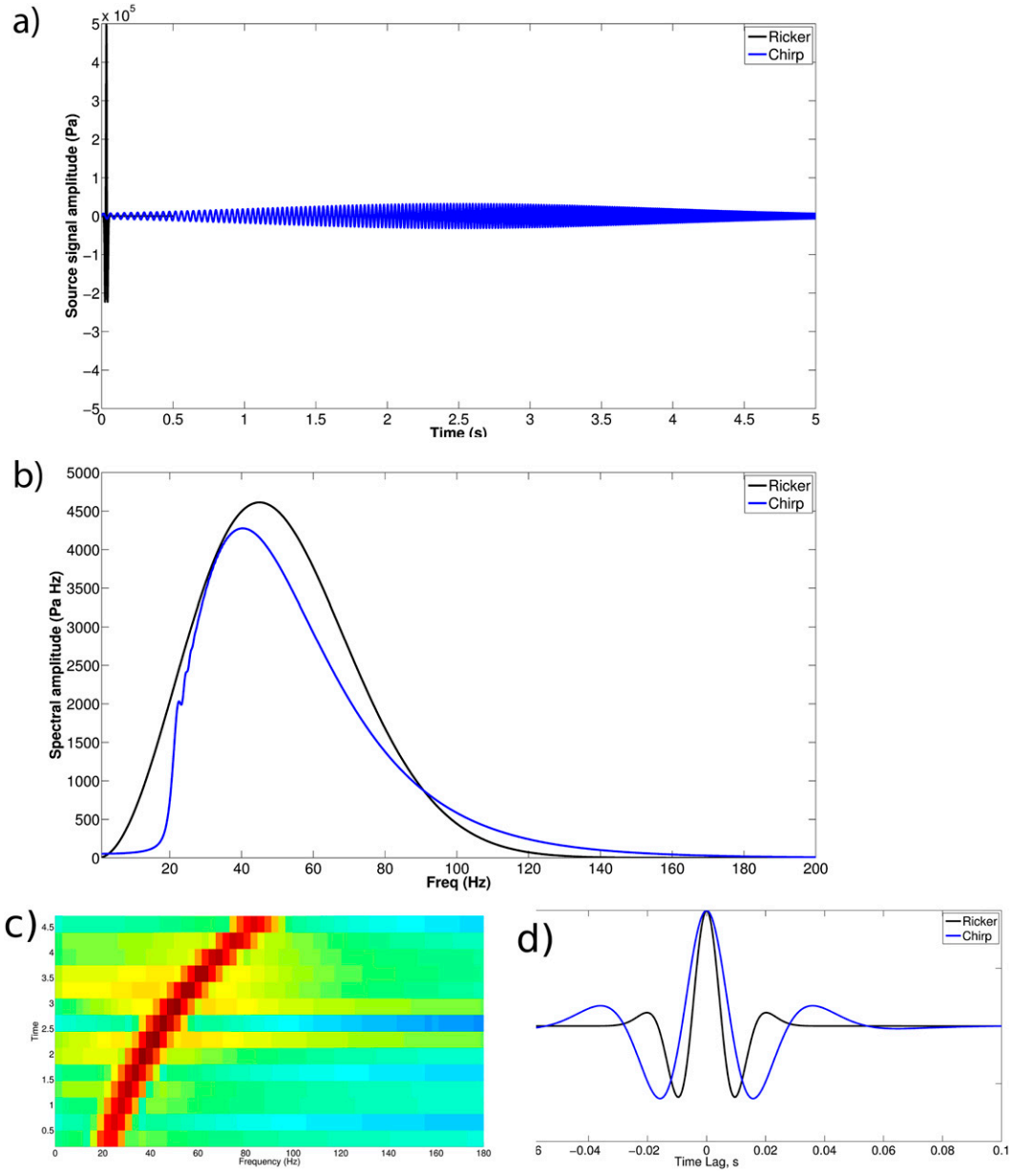

FIG. 1. The 234 dB relative to 1 μPa at 1 m Ricker wavelet (black) and 5-s exponential chirp of 208 dB relative to 1 μPa at 1 m with a Gaussian taper (blue) displayed as (a) time domain, (b) frequency domain, (c) chirp spectrogram, and (d) Klauder wavelets.

adding contiguous CMP into the same stacked trace. The advantage of increasing the fold is that the SNR increases and the drawback is that the lateral resolution decreases. The GO-LR-01 data were processed with a fold of 60 (a 2400-m-long streamer with 192 channels, 12.5-m distance between channels, and 20-m shot spacing), which provided an acceptable SNR of the stacked data (Fig. 4a). Because one of the interests for the new MCS system is increasing its portability, a shorter streamer is proposed in this work, with 100 channels separated by 5 m between them and a 20-m shot spacing. This geometry results in a nominal CMP spacing (lateral sampling) of 2.5 m. Considering this geometry, Eq. (4) yields a fold of 12, which would be 5 times smaller than the one of the GO-LR-01 data and would result in a low SNR. To achieve an acceptable SNR, we quadruple the fold to 48 by decreasing the lateral resolution down to 10 m by stacking four neighboring CMPs together.

Reducing the spacing between shots would also increase the fold; however, the time length of the chirp

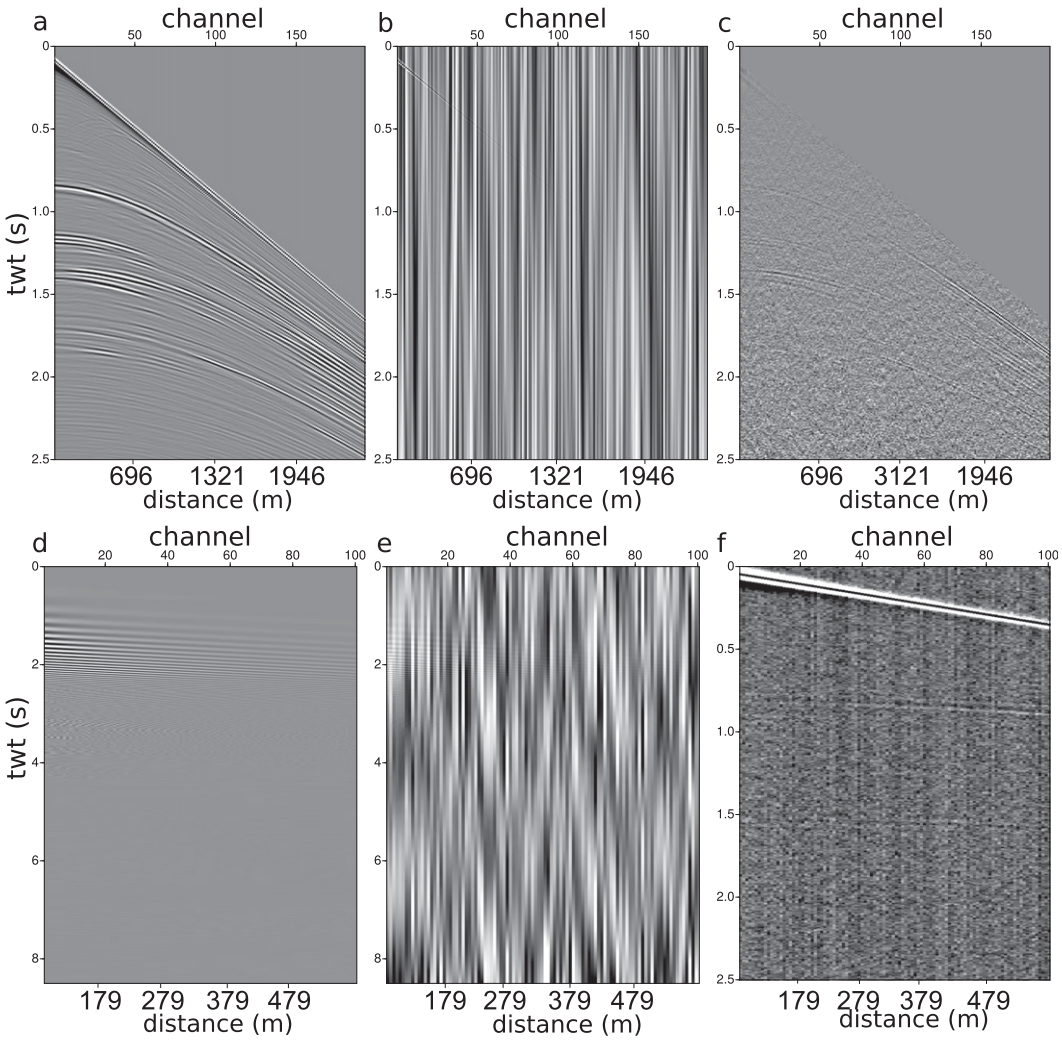

FIG. 2. Shot gather of 192 channels generated (a) with the Ricker wavelet of 234 dB relative to 1 μPa at 1 m, (b) with synthetic noise, and (c) after applying a frequency filter. Shot gather of 100 channels generated (d) with the 5-s exponential chirp wavelet of 208 dB relative to 1 μPa 1 at 1 m, (e) with synthetic noise, and (f) after correlating the data with the source wavelet and applying a frequency filter.

wavelet limits the minimum distance between shots. Considering the 5-s chirp and a water layer of 2 km, shots should be recorded during 7.5 s. Therefore, if the vessel moves at 4.5-kt speed (2.3 m s^{-1}), the minimum distance between shots should be ~17 m, which agrees with our 20-m shot spacing.

d. Noise model

To simulate scenarios that are as realistic as possible, the background noise to be added to the synthetic data is modeled following these three steps: (i) random amplitudes (absolute maximum amplitude) set independent for all channels and all shot gathers involved in the synthetic MCS experiment are generated; (ii) the random amplitude signals (white spectra) are convolved with real recorded noise in the ocean to obtain noise with realistic spectra; and (iii) spectral levels are set using the Wenz curves to obtain a medium noise level. Wenz (1962) gave a detailed analysis of the spectral characteristics of background oceanic noise from a variety of sources, including the earth's seismic activity, ship traffic, wind, waves, bubbles and spray, turbulence, and rain. The amplitude spectra of the background oceanic noise generated by the shipping intensity and the state of the sea, which mainly affect our acoustic data, were digitized from the results of Wenz (1962) in order to compare them with the generated synthetic noise (Fig. 3). This comparison illustrates that the noise considered in the present work has a frequency content within the range of realistic noise.

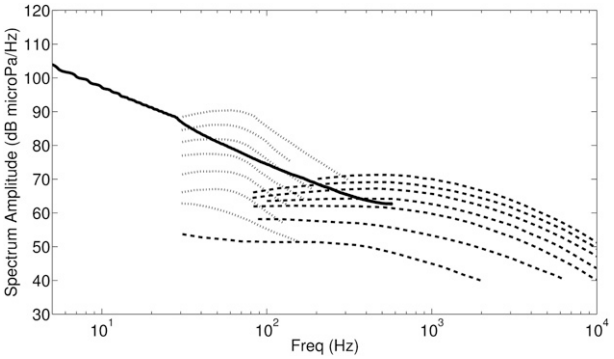

FIG. 3. Synthetic noise spectra used in this work (black and solid curve), shipping noise spectra for seven levels of intensity (Wenz 1962) (gray and spotted curves), and noise related to seven states of the sea, generated by the wind force (Wenz 1962) (gray and dashed curves).

3. Results

Data computed for the first experiment presented were produced using parameters (source frequency content and peak-to-peak amplitude, distances between shots and receivers, number of channels, first offset and fold) similar to those used in the GO-LR-01 profile acquired in the Gulf of Cadiz (northeast Atlantic Ocean). The acoustic synthetic source consists of a Ricker wavelet of 234 dB relative to 1 μPa at 1 m (500 000-Pa peak signal), with a frequency content in the range of 10–100 Hz (Fig. 1). To compare the synthetic and real data, we propagated the synthetic data through the sound speed model that was obtained by inverting the MCS data recorded along this line (Biescas et al. 2014). In particular, the section that we used is 5 km long and images the right edge of a meddy, which is a typical structure detected in this area that consists of a warm and salty rotating lens.

A comparison between the real (Fig. 4a) and synthetic experiments (Fig. 4b) shows remarkable similarity, with both displaying the same reflectors that correspond to the oceanic fine structure. The spectra of a part of the seismic section containing mainly reflected signal (S) and mostly noise (N) are calculated for both sections and the corresponding SNR is shown in the upper-right insets of Figs. 4a and 4b. The SNR of the real data is slightly lower than the one calculated from the synthetic experiment (peak at 1.5 vs peak at 2.2), probably due to additional noise in the real experiment generated by electronic effects in the hydrophones and the oscillations of the streamer and source near the sea surface. Overall, this comparison validates our methodology for generating realistic synthetic MCS experiments in the ocean and testing the effect of the involved variables.

The second synthetic experiment (Fig. 4c) simulates data that would be collected with the portable MCS system suggested in this work (Table 1) and characterized by a significantly lighter and shorter streamer that could be potentially installed and operated from a midsize oceanographic vessel. The source wavelet used in this experiment is a 5-s-long exponential chirp wavelet of 208 dB relative to 1 μPa at 1 m (a 25 000-Pa peak signal) with a Gaussian taper, which minimizes the sidelobes of the autocorrelation function of the chirp, and a frequency content of 20–100 Hz (Fig. 1).

The stacked section from these synthetic data (Fig. 4c) shows the meddy fine structure well, and the SNR is equivalent to that obtained using the impulsive source's system. The Ricker source is a signal 20 times stronger in amplitude than the chirp wavelet. However, as the chirp wavelet has a 5-s duration, the level of the total energy is similar to the one emitted by the Ricker pulse, resulting in similar levels of effectiveness in oceanic exploration.

The low acoustic reflection coefficients in the ocean ($\sim 10^{-4}$) create a significant trade-off between detectability and portability of the system. The system proposed was chosen from several tests that were conducted for this work. However, other combinations of parameters may give similar SNR by compensating between the different factors. Figure 5 shows two examples of unsuccessful systems, with SNR $\sim$1. These two examples were similar to the one proposed but have (i) a lower amplitude of the 5-s chirp, 200 dB relative to 1 μPa at 1 m; and (ii) a smaller stack fold, 12 instead of 48; and neither example allows for detection of the meddy fine structure with a suitable SNR.

4. Discussion and conclusions

MCS systems with air gun sources used for solid Earth applications have shown to be suitable for deep oceanic exploration; however, these systems require expensive instrumentation and vessels. The scientific community developing ocean seismic visualization is making a joint effort to find small- and midsize multichannel seismic systems that could be used to explore the physics of the ocean (Geli et al. 2009; Carniel et al. 2012; Piété et al. 2013; Ker et al. 2015), but the low reflectivity of the ocean ($R \sim 10^{-4}$) makes this goal challenging. In this work we propose the use of chirp wavelets emitted with a broadband sound projector source instead of classical air gun pulses.

We exemplify through numerical simulations that an oceanic thermohaline structure can be detected with similar SNR using an impulsive source of 234 dB relative to μPa 1 at 1 m (a 500 000-Pa peak signal) or equivalently a 5-s chirp source of 208 dB relative to μPa at 1 m (a 25 000-Pa peak signal). The chirp source can reduce the peak of the pressure signal 20 times by spreading the energy in

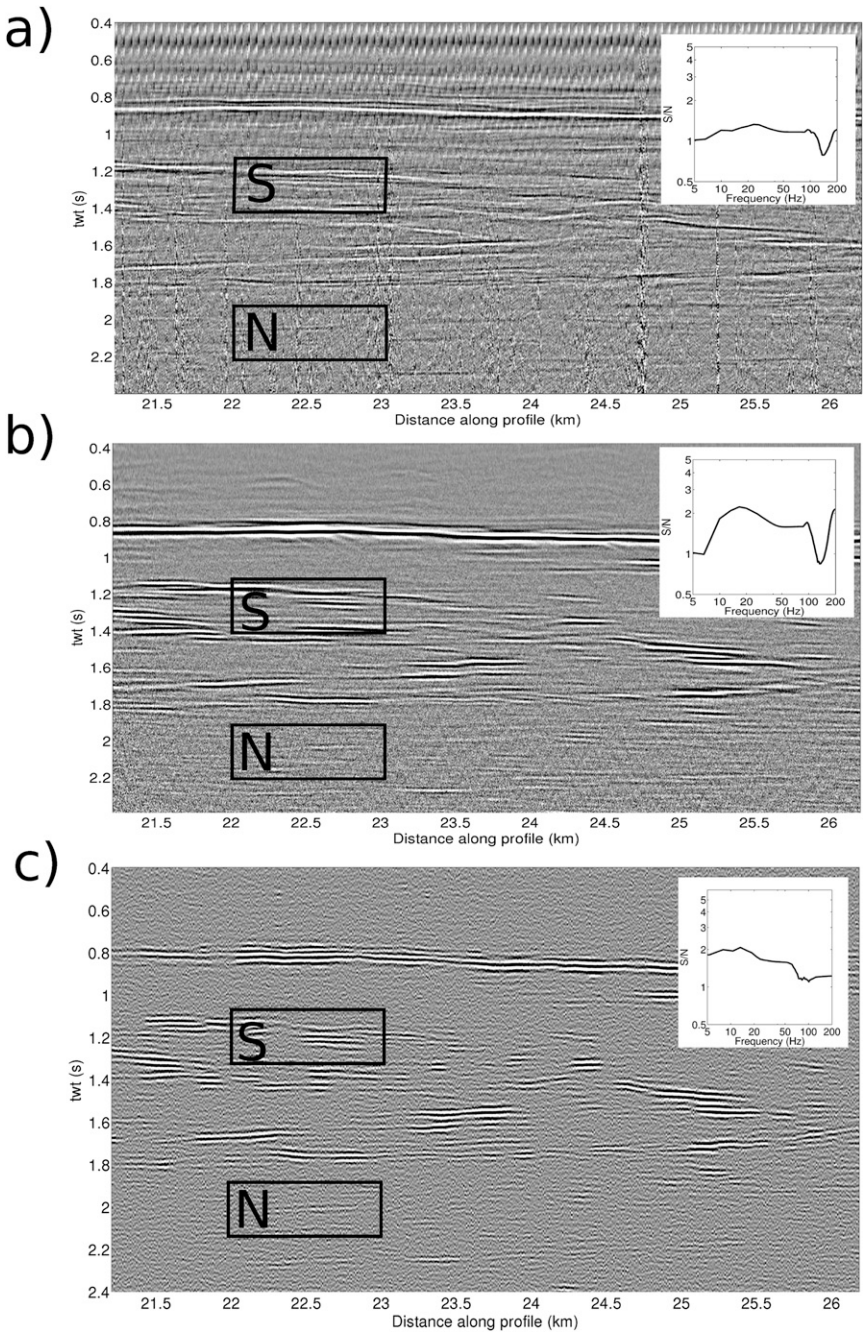

FIG. 4. (a) Stack section of 5 km long of the GO-LR-01 profile acquired in the GO survey (Gulf of Cadiz, northeast Atlantic Ocean, April–May 2006). (b) Stack section of the synthetic data generated with the 234 dB relative to 1 μPa at 1 m Ricker wavelet. (c) Stack section of the synthetic data generated with the 208 dB relative to 1 μPa 1 at 1 m 5-s exponential chirp wavelet. The upper-right white insets correspond to the SNR of the data within the two corresponding rectangles.

time. There is evidence that a swept signal with lower peak amplitude may have less impact on marine animals than a higher peak impulsive signal (Weilgart 2012). For example, considering the Ricker source, the radius of the exclusion zone for certain species (an area affected by more than 160 dB relative to 1 μPa) would be 5000 m. That means that, if these species were observed or detected with passive acoustic monitoring, closer than

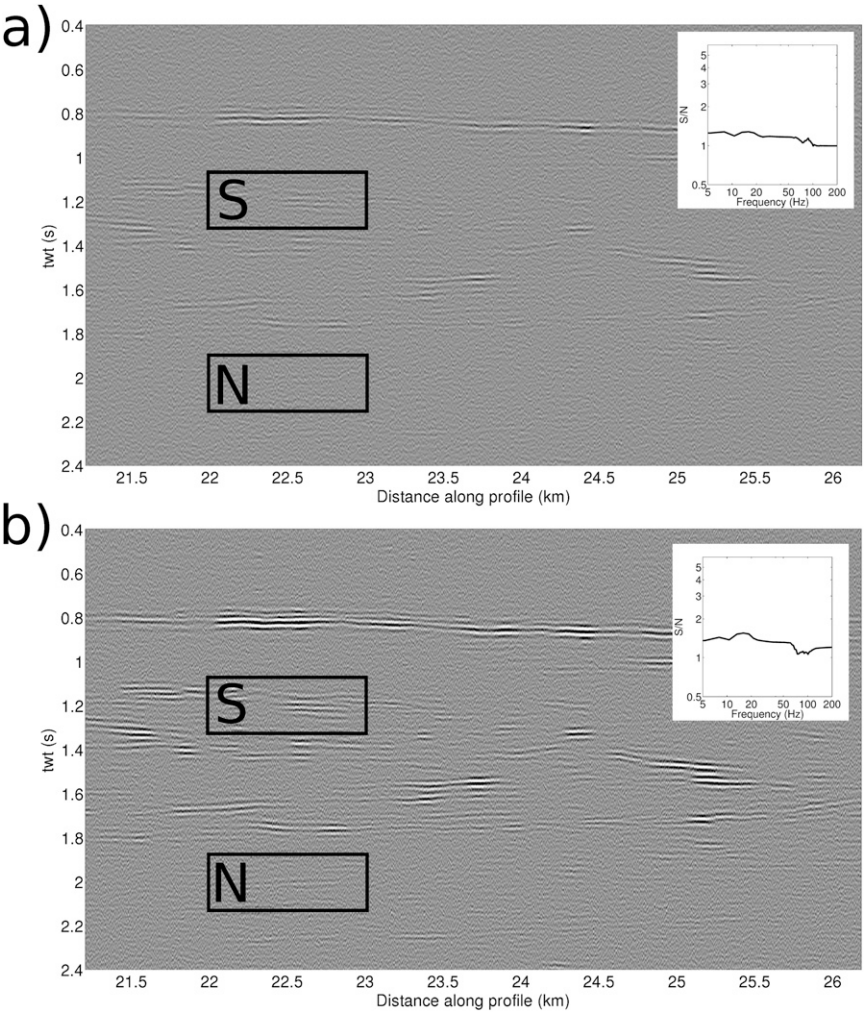

FIG. 5. Stack sections of the synthetic data generated with (a) 200 dB relative to 1 μPa at 1 m 5-s exponential chirp wavelet and processed with a fold equal to 60 and (b) 208 dB relative to 1 μPa at 1 m 5-s exponential chirp wavelet and processed with a fold equal to 15. The upper-right white insets correspond to the SNR of the data within the two corresponding rectangles.

5000 m to the air guns, these air guns had to be immediately shut down. Since the energy of the source decreases with the square of the distance, and since the energy is proportional to the square of the amplitude of the emitted signal, then the exclusion zone for the proposed system would be $A_R^2/d_R^2 = A_{\mathrm{Ch}}^2/d_{\mathrm{Ch}}^2$, $d_{\mathrm{Ch}} = \sqrt{A_{\mathrm{Ch}}^2 d_R^2/A_R^2} = 250$ m; thus, the mitigation distance for these species would be 20 times shorter than with the impulsive signal.

Regarding the frequency content of the source, it is known that the vertical resolution of acoustic data increases proportionally with the frequency content of the source. Consequently, a high-frequency seismic source would provide better vertical resolution. In spite of that, high-frequency sources ($f > 200$ Hz) tested in previous seismic oceanography (SO) surveys provided low SNR and a fine structure that was poorly detected with these sources (Geli et al. 2009; Ker et al. 2015), even though the background noise decreases when increasing frequencies (Fig. 3). To test frequencies higher than 100 Hz, we modeled two chirp wavelets through a synthetic medium obtained by expanding a single CTD profile to a horizontally uniform 2D sound speed model. This way, we produced a sound speed model with a vertical resolution of 1 m, which allowed us to test sources with a frequency content up to 375 Hz. Chirp wavelets were 5 s, 208 dB relative to 1 μPa at 1 m peak amplitude, and had a frequency content of 10–150 and 150–300 Hz (Fig. 6). The same level of synthetic background noise was added to the shots, and the comparison between both stack sections shows clearly that SNR decreases progressively as frequency increases (Fig. 6). Since the seismic signal is

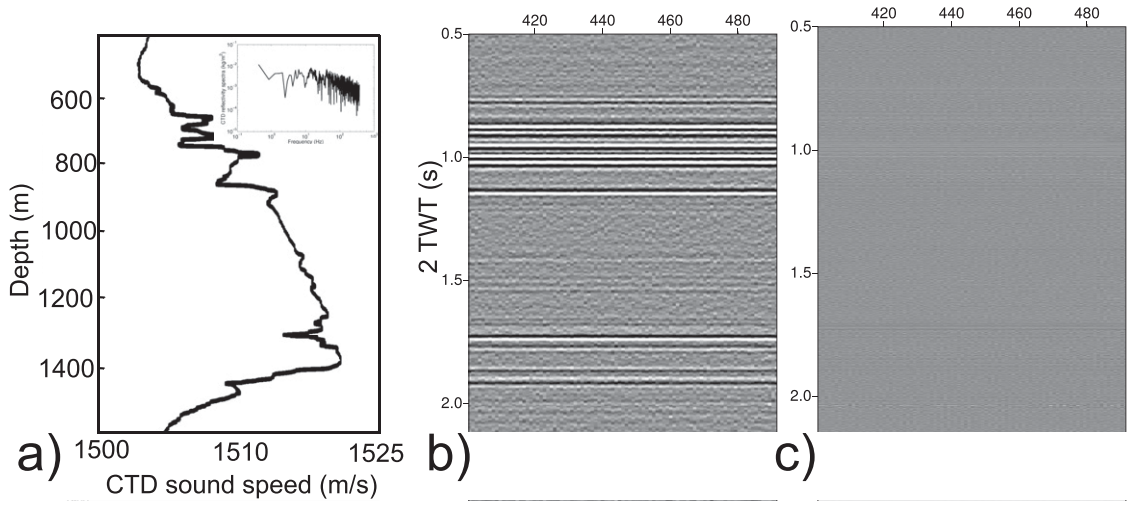

FIG. 6. (a) CTD sound speed profile used for the model and spectra of the reflectivity from the CTD data (upper-right inset). Stack sections obtained with the 5-s chirp, 205 dB relative to 1 μPa 1 at 1 m, and frequency content of (b) 10–150 and (c) 150–300 Hz.

the result of the convolution between the source wavelet and the reflectivity of the media, we have calculated the spectra of the reflectivity data from a CTD (upper-right inset in Fig. 6a) and it shows that oceanic reflectivity amplitude decreases with frequency, which supports the low SNR with high-frequency sources. The work presented by Ker et al. (2015) analyzes ocean reflectivity in terms of the frequency emitted from the source and the thickness of the thermocline to be detected, and corroborates that the signal amplitude decreases with increasing frequency regardless of the thermocline's thickness. Nevertheless, the optimal frequency content remains an open question and will strongly depend on the fine structure to be detected in each single experiment.

Problems regarding phase dispersion caused by the Doppler effect have been described in the use of marine vibrators (Dragoset 1988). We may note that even though dips in oceanic reflectors are generally very smooth, this effect would increase by increasing the frequency bandwidth and duration of the sweep, which should be taken into account in the design of the pulse.

The system that we propose in this work compensates for a shorter streamer and relatively low chirp source amplitude with a longer time duration. It would provide thermohaline information of the full-depth water column and along lateral distances of hundreds of kilometers in the ocean, with lateral and vertical resolutions on the order of $O(10)$ m. This proposed system could be the starting point for the development of an ocean-specific low-frequency acoustic projection system for physical oceanography.

Acknowledgments. The first author's work has been supported by the European Commission through Marie Curie Actions FP7-PEOPLE-2010-IOF-271936 and FP7-PEOPLE-2012-COFUND-600407. This work has been done in the framework of the Spanish project POSEIDON (CTM2010-25169) and the Italian National Flagship Programme RITMARE (Programma Nazionale della Ricerca 2011-2013 MIUR). We want to acknowledge the team of GO project funded by the EU (015603-GO-STREP).

REFERENCES

Biescas, B., V. Sallarès, J. Pelegrí, F. Machín, R. Carbonell, G. Buffett, J. Dañobeitia, and A. Calahorrano, 2008: Imaging meddy finestructure using multichannel seismic reflection data. *Geophys. Res. Lett.*, **35**, L11609, doi:10.1029/2008GL033971.

——, L. Armi, V. Sallarès, and E. Gràcia, 2010: Seismic imaging of staircase layers below the Mediterranean undercurrent. *Deep-Sea Res. I*, **57**, 1345–1353, doi:10.1016/j.dsr.2010.07.001.

——, B. Ruddick, M. Nedimović, V. Sallarès, G. Bornstein, and J. Mojica, 2014: Recovery of temperature, salinity, and potential density from ocean reflectivity. *J. Geophys. Res. Oceans*, **119**, 3171–3184, doi:10.1002/2013JC009662.

Bornstein, G., B. Biescas, A. Sallares, V. Bower, and J. Mojica, 2013: Direct temperature and salinity acoustic full waveform inversion. *Geophys. Res. Lett.*, **40**, 4344–4348, doi:10.1002/grl.50844.

Buffett, G., B. Biescas, J. Pelegrí, F. Machín, V. Sallarès, R. Carbonell, D. Klaeschen, and R. Hobbs, 2009: Seismic reflection along the path of the Mediterranean Undercurrent. *Cont. Shelf Res.*, **29**, 1848–1860, doi:10.1016/j.csr.2009.05.017.

Carniel, S., A. Bergamasco, J. Book, R. W. Hobbs, M. Sclavo, and W. Wood, 2012: Tracking bottom waters in the Southern

Adriatic Sea applying seismic oceanography techniques. *Cont. Shelf Res.*, **44**, 30–38, doi:10.1016/j.csr.2011.09.004.

Cohen, J., and J. Stockwell, 2003: CWP/SU: Seismic Unix release No. 36: A free package for seismic research and processing. Center for Wave Phenomena, Colorado School of Mines, 153 pp.

Dragoset, W., 1988: Marine vibrators and the Doppler effect. *Geophysics*, **53**, 1388–1398, doi:10.1190/1.1442418.

Flandin, P., 2001: The frequency and chirps. *Wavelet Applications VIII*, H. H. Szu et al., Eds., International Society for Optical Engineering (SPIE Proceedings, Vol. 4391), 161–175, doi:10.1117/12.421196.

Geli, L., E. Cosquer, R. Hobbs, D. Klaeschen, C. Papenberg, Y. Thomas, C. Menesguen, and B. Hua, 2009: High resolution seismic imaging of the ocean structure using a small volume airgun source array in the Gulf of Cadiz. *Geophys. Res. Lett.*, **36**, L00D09, doi:10.1029/2009GL040820.

Hobbs, R., D. Klaeschen, V. Sallarès, K. Vsemirnova, and C. Papenberg, 2009: Effect of seismic source bandwidth on reflection sections to image water structure. *Geophys. Res. Lett.*, **36**, L00D08, doi:10.1029/2009GL040215.

Holbrook, W., I. Fer, R. Schmitt, D. Lizarralde, J. Klymak, L. Helfrich, and R. Kubiche, 2013: Estimating oceanic turbulence dissipation from seismic images. *J. Atmos. Oceanic Technol.*, **30**, 1767–1788, doi:10.1175/JTECH-D-12-00140.1.

Hua, B., C. Ménesguen, S. Le Gentil, R. Schopp, B. Marsset, and H. Aiki, 2013: Layering and turbulence surrounding an anticyclonic oceanic vortex: In situ observations and quasi-geostrophic numerical simulations. *J. Fluid Mech.*, **731**, 418–442, doi:10.1017/jfm.2013.369.

Ker, S., Y. Le Gonidec, L. Marié, Y. Thomas, and D. Gibert, 2015: Multiscale seismic reflectivity of shallow thermoclines. *J. Geophys. Res. Oceans*, **120**, 1872–1886, doi:10.1002/2014JC010478.

Kormann, J., P. Cobo, M. Recuero, B. Biescas, and V. Sallarès, 2009: Modelling seismic oceanography experiments by using first- and second-order complex frequency shifted perfectly matched layers. *Acta Acust. Acust.*, **95**, 1104–1111, doi:10.3813/AAA.918242.

——, ——, B. Biescas, V. Sallarès, C. Papenberg, M. Recuero, and R. Carbonell, 2010: Synthetic modelling of acoustical propagation applied to seismic oceanography. *Geophys. Res. Lett.*, **37**, L00D90, doi:10.1029/2009GL041763.

Ménesguen, C., B. Hua, C. Papenberg, D. Klaeschen, L. Géli, and R. Hobbs, 2009: Effect of bandwidth on seismic imaging of rotating stratified turbulence surrounding an anticyclonic eddy from field data and numerical simulations. *Geophys. Res. Lett.*, **36**, L00D05, doi:10.1029/2009GL039951.

Papenberg, C., D. Klaeschen, G. Krahmann, and R. Hobbs, 2010: Ocean temperature and salinity inverted from combined hydrographic and seismic data. *Geophys. Res. Lett.*, **37**, L04601, doi:10.1029/2010GL042115.

Piété, H., L. Marié, B. Marsset, Y. Thomas, and M.-A. Gutscher, 2013: Seismic reflection imaging of shallow oceanographic structures. *J. Geophys. Res. Oceans*, **118**, 2329–2344, doi:10.1002/jgrc.20156.

Pinheiro, L., H. Song, B. Ruddick, J. Dubert, I. Ambar, K. Mustafa, and R. Bezerra, 2010: Detailed 2-D imaging of the Mediterranean outflow and meddies off W Iberia from multichannel seismic data. *J. Mar. Syst.*, **79**, 89–100, doi:10.1016/j.jmarsys.2009.07.004.

Quentel, E., X. Carton, M.-A. Gutscher, and R. Hobbs, 2010: Detecting and characterizing mesoscale and submesoscale structures of Mediterranean water from joint seismic and hydrographic measurements in the Gulf of Cadiz. *Geophys. Res. Lett.*, **37**, L06604, doi:10.1029/2010GL042766.

Ruddick, B., 2003: Sounding out ocean fine structure. *Science*, **301**, 772–777, doi:10.1126/science.1086924.

Sallarès, V., B. Biescas, G. Buffett, R. Carbonell, J. Dañobeitia, and J. Pelegrí, 2009: Relative contribution of temperature and salinity to ocean acoustic reflectivity. *Geophys. Res. Lett.*, **36**, L00D06, doi:10.1029/2009GL040187.

Smith, K., and R. Ferrari, 2009: The production and dissipation of compensated thermohaline variance by mesoscale stirring. *J. Phys. Oceanogr.*, **39**, 2477–2501, doi:10.1175/2009JPO4103.1.

Vsemirnova, K., R. Hobbs, and P. Hosegood, 2012: Mapping turbidity layers using seismic oceanography methods. *Ocean Sci.*, **8**, 11–18, doi:10.5194/os-8-11-2012.

Weilgart, L., 2012: Are there technological alternatives to air guns for oil and gas exploration to reduce potential noise impacts on cetaceus? *The Effects of Noise on Aquatic Life*, A. Popper and A. Hawkins, Eds., Advances in Experimental Medicine and Biology, Vol. 730, Springer New York, 605–607, doi:10.1007/978-1-4419-7311-5_137.

Wenz, G., 1962: Acoustic ambient noise in the ocean: Spectra and sources. *J. Acoust. Soc. Amer.*, **34**, 1963–1956, doi:10.1121/1.1909155.

Yilmaz, O., 2001: *Seismic Data Analysis: Processing, Inversion, and Interpretation of Seismic Data*. 2nd ed. Society of Exploration Geophysicists, 2027 pp.